Reconciling asymmetry observations in the permeability tensor of digital rocks with symmetry expectations

Lesueur, Martin; Guével, Alexandre; Poulet, Thomas

Important note
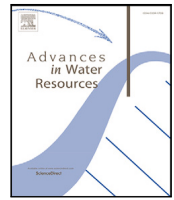To cite this publication, please use the final published version (if applicable).
Please check the document version above.

Reconciling asymmetry observations in the permeability tensor of digital rocks with symmetry expectations

Martin Lesueur [a,b,*], Alexandre Guével [c], Thomas Poulet [d]

[a] *School of Earth Sciences, University of Western Australia, Perth, Australia*
[b] *Civil Engineering and Geosciences, Delft University of Technology, Delft, Netherlands*
[c] *Civil and Environmental Engineering, Duke University, Durham, USA*
[d] *CSIRO Mineral Resources, Perth, Australia*

ARTICLE INFO

ABSTRACT

Modelling anisotropic flow in rocks requires their full permeability tensor. While theories derived from the upscaling of Stokes flow to Darcy's law may justify the tensor symmetry, homogenisations from micro-scale rock samples often return a non-zero level of asymmetry. Since most studies dismiss these controversial observations as numerical errors, this contribution looks more closely at the physical possibility of such behaviour. Asymmetry of the permeability tensor, which induces a rotatory flow, is manifested at the micro-scale by tortuous streamlines. Conversely, when considering a larger scale – above the Representative Elementary Volume for permeability – these tortuous paths do not statistically affect the flow direction any longer. At this point, the homogenisation of Stokes flow to Darcy's law reaches its domain of validity. We show that the asymmetry in the permeability tensor vanishes for this scale separation, regardless of the choice of boundary conditions unlike previously thought, if the boundary layer effect is disregarded.

1. Introduction

Permeability is arguably the most important rock property to determine for subsurface energy and resources engineering applications, for example in the fields of groundwater resources, petroleum engineering or geothermal energy, which all critically depend on the behaviour of fluid flow through porous rocks. In its most generic form, the permeability of an anisotropic medium is expressed as a tensor, yet it has for a long time been mostly characterised by its diagonal components only, defined in the oil and gas industry as horizontal and vertical permeabilities. The possibility of determining its off-diagonal components was only enabled much later with the development of Digital Rock Physics (see Dvorkin et al., 2008; Blunt et al., 2013). This approach allows to numerically determine the rock permeability through upscaling of the flow simulated in a Representative Elementary Volume (REV) from its digitalised microstructure. Note that reaching REV of the permeability tensor implies convergence of each of its components. Every component of the tensor can be derived by imposing some flow in a specific direction and measuring the resulting effective permeability along one of the three axes. This workflow provides the full permeability tensor, which is necessary for modelling anisotropic flow occurring in unconventional resources for instance.

On top of the flow anisotropy observed in some porous media, an even more remarkable aspect has sometimes been detected during the

evaluation of the permeability tensor: its asymmetry. This was reported for instance on cross-bedded reservoirs (Zijl and Stam, 1992; King, 1993), fracture networks (Long et al., 1982; Sagar and Runchal, 1982; Baghbanan and Jing, 2007; Lang et al., 2014; Sedaghat et al., 2019) or rock microstructures (Manwart et al., 2002; Guibert et al., 2015a,b; Thovert and Mourzenko, 2020).

However, this observation raises controversy. Indeed, it has been shown from homogenisation theories, such as those based on asymptotic expansions (Auriault, 1991; Auriault et al., 2000), that the permeability, defined by Darcy's law, has to be symmetric, provided that scale separation is satisfied (Lasseux and Valdés-Parada, 2017). Thereby, the asymmetry of the permeability tensor is often regarded as a numerical error stemming from the homogenisation procedure. For example, Guibert et al. (2015a) showed for a periodic synthetic porous medium that most classic boundary conditions result in permeability asymmetry. For this reason, numerical modellers have been developing methods to remove or at least reduce this asymmetry (Sanchez-Palencia, 1982; Durlofsky, 1991; Lang et al., 2014; Guibert et al., 2015a; Gerke et al., 2019). They most often amount to enforcing the assumptions underpinning homogenisation (even though they may not be satisfied in reality), for instance by enforcing periodicity of the numerical domain through translation or symmetrisation, or by employing

periodic boundary conditions. Note that the classical set-up is meant to reproduce the experimental conditions of the experimental permeameter, i.e. with no-slip boundary conditions on the external boundaries. Periodic boundary conditions can either be imposed on symmetric domains or embedded subdomains, the latter being a technique that embeds the domain in an equivalently permeable medium (Stroud, 1998; Guibert et al., 2015a) onto which periodic boundary conditions are applied. In that case, while periodicity is not completely ensured in the embedded subdomain, asymmetry is greatly reduced. Guibert et al. (2015a) and Gerke et al. (2019) propose a review of these different methods.

Enforcing periodicity in that fashion is, however, artificial, since induced by special numerical treatments. Specifically, Gerke et al. (2019) showed that these numerical schemes could not reproduce the natural conditions that would surround the rock sample considered, and even alter the real flow magnitude or direction. Furthermore, Thovert and Mourzenko (2020) showed that all boundary conditions only affect a finite layer at the boundary of the computational domain. Based on this concept, the consideration of a subdomain away from this boundary layer is the safest practice to remove the artificial boundary effect. Going further, Thovert and Mourzenko (2020) proved that homogenisation procedures run on such a subdomain resulted in the same permeability tensor regardless of the boundary conditions employed. Interestingly in that case, the homogenised tensor was shown to remain asymmetric, reinforcing the idea that the numerical periodicity enforced is artificial.

Rather than looking at permeability tensor asymmetry from a numerical error perspective, we propose to focus on its physical implication: the flow becomes rotatory, i.e. follows curved streamlines. Indeed, it was derived by Stokes (1851) in the context of heat conduction, and reminded by Truesdell (1984, p. 113), that the flow due to a gradient driving force follows curved streamlines whenever the antisymmetric part of the associated diffusion tensor is non-zero. Such rotatory flow can also directly be induced by the rotation of the porous medium, whereby fictitious forces (Coriolis, centrifugal, Euler) appear at the pore scale. The homogenisation of the latter through asymptotic expansion yields a non-zero K_a (Auriault et al., 2000). A rotatory Darcy flow can also occur when the microstructure lacks reflectional symmetry, as conceived of by Koch and Brady (1987) (wherein the gradient of pressure is replaced by a gradient of concentration).

Considering the dependency of permeability on the physical length-scale of interest, it is common to see permeability values converge with increasing sample size as it reaches the REV at that scale, when scale separation is met, before diverging again when the sample size increases past the threshold marking the start of the next length-scale (Veveakis and Regenauer-Lieb, 2015). As such, permeability studies are usually confined to specific scales, either focusing on the microstructure ($\sim \mu m$), rock plugs ($\sim cm$) or fractured media ($\sim hm$). Interestingly, the presence of asymmetry in the permeability tensor is already an accepted concept in hydrogeology at that larger scale, like in cross-bedded reservoirs or fracture networks as mentioned previously. Additionally, some studies showed that this asymmetry vanishes when reaching the REV size (Long et al., 1982; Baghbanan and Jing, 2007; Pouya and Fouché, 2009). The deviation from the classical symmetric Darcy law is therefore attributed to violating the homogenisation assumptions, i.e. scale separation and domain's periodicity or, equivalently for homogenisation purposes, randomness (Auriault, 1991). At the micro-scale, however, since permeability asymmetry has traditionally been considered as an error, this type of analysis is simply missing.

In this contribution, we propose to fill in this gap and study permeability asymmetry for porous media at the micro-scale, where scale separation is not guaranteed since we operate too close to the grain length-scale. We suggest observing the asymmetry from a new perspective, away from artificial boundaries and look at the parameters of the homogenisation procedure that can influence it. Those parametric studies are first made for simpler porous media in Section 2. Then, the expected theoretical behaviour is assessed on real rock microstructures in Section 3.

2. Theoretical study

Grain shape, including roughness, has a strong influence on permeability estimation from rock microstructures (Beard and Weyl, 1973; Cox and Budhu, 2008; Torskaya et al., 2013). Sources of heterogeneity such as this one could also be expected to produce or increase the asymmetry of the permeability tensor. In this first section, we check therefore for the presence of asymmetry on simple structures where this particular feature is excluded, which can only be achieved in a Random Close Packing (RCP) of perfectly round spheres.

2.1. Material and methods

In order to obtain results representative of the porous medium selected, we need to consider a number of spheres in our computational domain large enough to reach the REV size of permeability. Using the OpenMC package (Romano et al., 2015), we generate a 3D sample that contains in average 80 spheres of constant radius per direction. We assume this amount to be past REV size for permeability, which is verified in the following subsections. In order to reduce the memory consumption of simulations on such a large sample, we consider only a 2D cross section of the RCP. Marafini et al. (2020) showed that the added flow path connectivity obtained when considering the third dimension only amounts to decreasing the size of the REV. Still, the nature of the flow remains unchanged and a 2D analysis remains sufficient to investigate the asymmetry evolution until REV. The selected slice is meshed with triangles in Gmsh (Geuzaine and Remacle, 2009) at a given mesh resolution. The cross section obtained can be observed in Fig. 1, with the sliced spheres appearing in white.

The permeability tensor is obtained from the homogenisation of Stokes flow, solved within the pore space of the RCP (Lesueur et al., 2017). At the pore–grain interface, classic no-slip boundary conditions are imposed. The selection of the external boundary conditions has been shown by Thovert and Mourzenko (2020) not to influence the results. Therefore, we decide to specifically enforce slip boundary conditions – i.e. the normal component of the fluid velocity at the boundary is null – on the walls to revisit a set of boundary conditions from the study of Guibert et al. (2015a), for which the symmetry of the permeability tensor was never reached, even for a periodic synthetic porous medium at REV. Two Stokes simulations are needed to obtain every component of the permeability tensor (in 2D), i.e. one for each direction (x and y indicated respectively by exponents 1 and 2). The flow is resulting from a pressure gradient imposed across the domain, denoted respectively as $\overline{\nabla P_x^1}$ and $\overline{\nabla P_y^2}$ for the two simulations, following notations from Guibert et al. (2015a). The velocity field simulated with the pressure gradient $\overline{\nabla P_x^1}$ can be visualised in Fig. 1. For each simulation, every directional component of that velocity field is averaged volumetrically (denoted by $\langle \cdot \rangle$), providing overall the four values ($\langle v_x^1 \rangle, \langle v_y^1 \rangle$) and ($\langle v_x^2 \rangle, \langle v_y^2 \rangle$). Similarly, we also average the pressure gradient in the transversal direction, from which we can extract $\overline{\nabla P_y^1}$ and $\overline{\nabla P_x^2}$. The full permeability tensor is then obtained using all these quantities by formulating Darcy's law, as

$$\begin{pmatrix} K_{xx} & K_{xy} \\ K_{yx} & K_{yy} \end{pmatrix} \begin{pmatrix} \overline{\nabla P_x^1} & \overline{\nabla P_x^2} \\ \overline{\nabla P_y^1} & \overline{\nabla P_y^2} \end{pmatrix} = \mu \begin{pmatrix} \langle v_x^1 \rangle & \langle v_x^2 \rangle \\ \langle v_y^1 \rangle & \langle v_y^2 \rangle \end{pmatrix}. \tag{1}$$

We note that the velocity in Eq. (1) refers to the superficial velocity, which is obtained by multiplying the velocity field obtained with the simulation of Stokes flow by the porosity.

For Eq. (1) to yield values of permeability, the meshed pore space needs to be above the percolation threshold. For the purpose of this study, it is unnecessary to compute that threshold precisely and percolation is more simply assessed by comparing the pressure gradient on the subsample with the average value for all simulations on that sample. When the pressure gradient of a sub-sample is too far away from the average value, percolation is deemed not to exist. For each sample

analysed in this work, the cut-off values were selected by plotting the distribution of pressure gradients for all subsamples considered, which showed clear discrepancies (and often a gap) between the values close to the average and the extremum values.

By definition a permeability tensor **K** is asymmetric if there exists a pair of indices (i, j) where $K_{ij} \neq K_{ji}$. In order to study the evolution of this property in digital rocks, it is convenient to define a quantitative asymmetry index. In this article, we use the normalised asymmetry vector whose components are defined as

$$\frac{K_{ij} - K_{ji}}{2 \, K_{mean}}, \, for \, i > j. \tag{2}$$

The vector is normalised by K_{mean} which is the mean of the diagonal components of the permeability tensor (shortened to mean permeability in the rest of the paper). In 2D, this is a scalar for $(i, j) = (x, y)$. In 3D, it is a vector of xy, xz and yz components. A scalar index can easily be derived subsequently by taking the norm of that vector. For instance, Thovert and Mourzenko (2020) defines it as $\sum_{i<j} [(K_{ij} - K_{ji})/2]^2$. While such an index has the advantage of being a scalar that captures the magnitude of the asymmetry in any dimension, we find it more convenient in our study to work with the vector itself. Indeed, its components can be positive or negative and the sign indicates the direction towards which the flow is deviated by the rotational element. In the rest of the paper for simplification, the term *K-asymmetry* will refer directly to the component(s) of the vector of the asymmetry of the permeability tensor.

As Thovert and Mourzenko (2020) demonstrated, one should check the extent of the boundary effect in the sample to carefully select a size fraction of the computational domain on which to postprocess the results, i.e. homogenise the permeability tensor. For that purpose, the permeability computed on the RCP sample presented in Fig. 1 (normalised by the final value) is plotted versus the size fraction of the computational domain considered for the homogenisation (growing from the centre of the full sample) in Fig. 2a. Note that the RCP is isotropic so we can plot directly the mean permeability instead of one specific diagonal component. Similarly to what was observed by Thovert and Mourzenko (2020), the permeability displays a clear change of behaviour past the consideration of a volume fraction larger than ∼90%. After having reached a constant value, a sharp increase is noticed until considering the full computational domain. We can therefore confirm the existence of a boundary layer, in which boundary effects can be perceived. Consequently, we recommend like Thovert and Mourzenko (2020) to postprocess results on a fraction of the total computational domain for more representative results. In this article, we select a maximum of 90% of the domain.

For that same RCP sample, Fig. 2b shows the corresponding K-asymmetry, which displays stronger variations than the mean permeability. It even changes sign sporadically and finally fluctuates around a non-zero value. If this result can be trusted, it would confirm the observation of K-asymmetry in digital rocks, and we could declare that its existence is not due to any grain shape heterogeneity as we considered an idealisation of porous media with perfectly round spheres. In the following section, we therefore investigate whether the K-asymmetry observed can be attributed to a simple numerical error, as it is commonly believed in the literature.

2.2. Mesh convergence

It is important to differentiate the various levels of convergence involved in this study. The first, at the highest level, refers to the physical size of the sample analysed and is used to identify the REV size, i.e. the minimum number of spheres required in the case of a RCP, for the property of interest to be representative. The second level corresponds to the mesh resolution used to simulate a given sample, i.e. to the number of numerical elements used for a fixed number of spheres in the case a RCP. In the third level we regroup all the numerical parameters related to the numerical convergence of the simulator

towards a solution, for a fixed physical size of the sample and given mesh resolution. In this contribution, all simulations were run using an absolute tolerance of 1e-9 on the residual to assess convergence, which ensures a satisfactory rigour level for the third level. Before searching for the REV size (first level), mesh convergence has to be established for accurate results (second level). The resolution of the mesh is increased directly via the length of the triangles in Gmsh. Fig. 3a shows the evolution of the mean permeability with the number of elements in the mesh. We observe visually an asymptotic convergence and set the mesh convergence at 5M (5e6) elements since it falls below one percent of deviation from the value with twice as many elements.

In parallel, Fig. 3b displays the evolution of the K-asymmetry with the mesh convergence and shows that the K-asymmetry rapidly converges to its final value. In our study it is already reached below 1M elements. We note that the final value obtained after removing numerical error, i.e. after having reached mesh convergence is not null. This proves that the K-asymmetry is not linked to a numerical error as commonly believed.

2.3. Representative elementary volume

Having confirmed the mesh convergence, we now search for the REV of permeability for the RCP. The REV is obtained when the mean permeability converges to a fixed value with increasing the sampling size. For this, a subsample of the computational domain of Fig. 1 is selected at a given position in the sample. Properties needed to solve for Eq. (1) are averaged on this subsample, and the full tensor of permeability is calculated. The process is repeated after increasing the subsample size until it reaches the full sample size. In order to improve the statistical representativeness, the process is repeated from different starting positions in the sample. We select growing subsamples from the centre and the four corners (outside the boundary layer). Unfortunately, an overlap of the different subsamples considered exists past a subdomain relative size of ≈0.45. Furthermore, at a subdomain size of 0.9, every subsample is the same. In order to keep statistical representativeness in the study, a second RCP is considered, generated exactly in the same manner with a different seed. Another set of curves is computed and added to the existing pool. From the obtained dataset, the average of the mean permeability and its fluctuations (range of values) are plotted in Fig. 4a. Past a size of 0.2, we observe that fluctuations consistently decrease with increasing subsample size. This regime corresponds to the scale of Statistical REV (Zhang et al., 2000), where the fluctuations are bounded and some interpretations can already be made. Eventually, the REV size is obtained above a size fraction of 0.75, after which the fluctuations in magnitude are negligible.

The corresponding evolution of the K-asymmetry is plotted in Fig. 4b. The K-asymmetry displays a behaviour similar to the mean permeability, converging rapidly to a steady value, which seems to be zero, or is at least undeniably negligible at the scale of the non-zero K-asymmetry of Fig. 4b. Given the ongoing narrowing of the fluctuation cone at a size of 0.9, the REV seems not to have been reached yet, but it is expected to occur soon after.

Interestingly, while we confirmed the existence of K-asymmetry in porous media at the micro-scale from the computation on one sample of RCP, shown in Fig. 2, we demonstrate that the average value when considering a large number of samples is zero, proving the statistical non-existence of the K-asymmetry in porous media. This result allows to reconcile those previous observations of K-asymmetry in porous media with upscaling theories where we find it verified for an REV of the porous medium. Note that reaching that size is also a necessary assumption for the validity of Stokes flow homogenisation to Darcy's law. Furthermore, we obtain a symmetric permeability tensor for a set of boundary conditions previously shown to only produce K-asymmetry (Guibert et al., 2015a), which proves that the issue is not about enforcing the periodicity with special numerical methods but
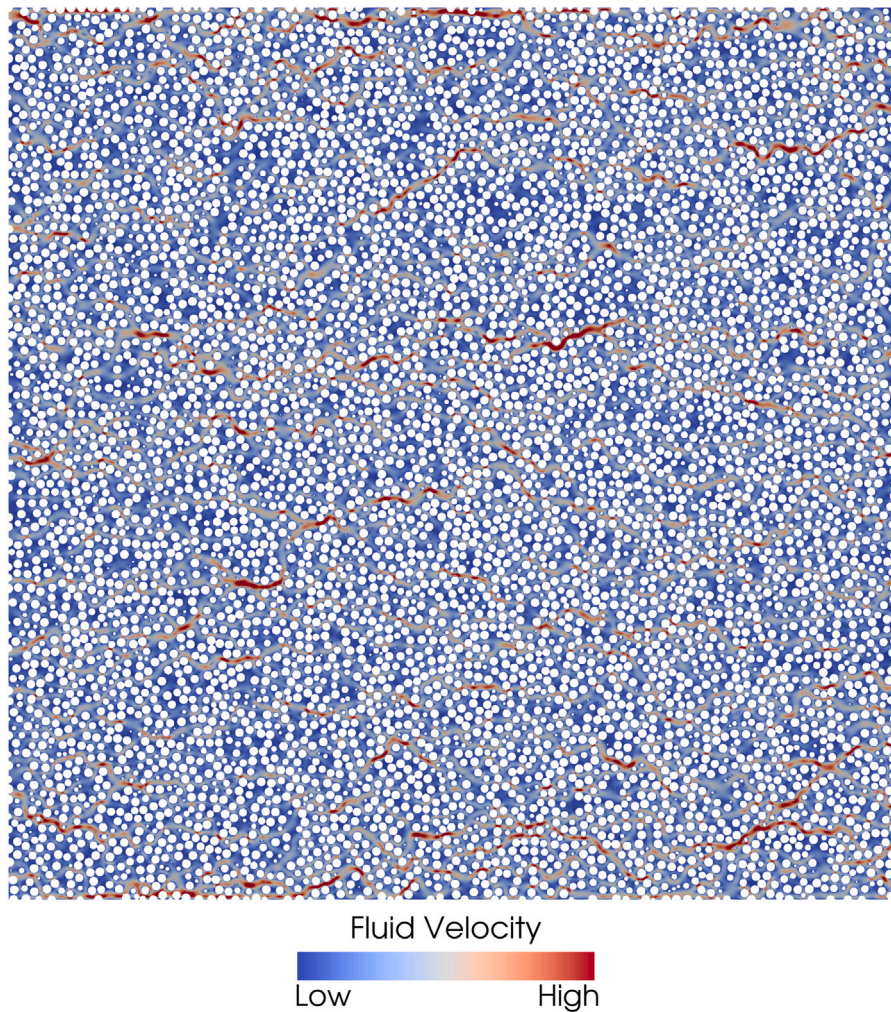
Fig. 1. Fluid velocity magnitude in a 2D cross section of a random close packing of spheres. The cross section cuts through 7100 spheres.
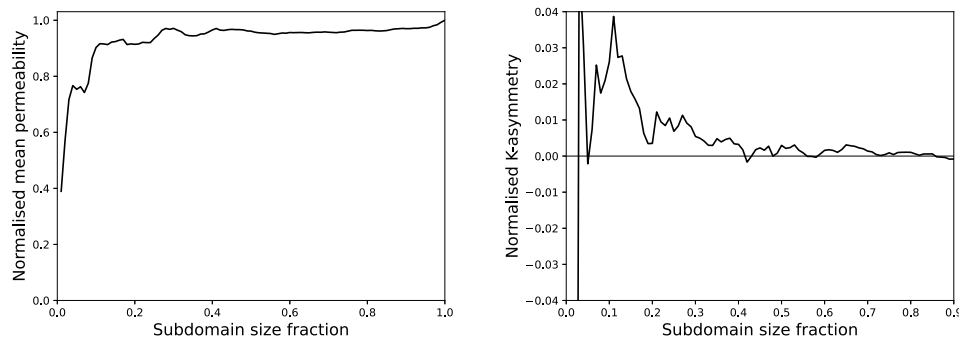

Fig. 2. Evolution of the mean permeability and K-asymmetry on subsamples growing from the centre position, for two RCP samples, including the one of Fig. 1.

instead, to assess the homogenised permeability tensor away from the boundaries.

This result can be understood in light of the flow rotation added by the K-asymmetry. In a random medium such as the RCP, the chances that the tortuous flow path through the structure generates a slight rotation towards either one direction or the other (corresponding to either positive or negative values of the K-asymmetry) are equal. This means that given a large enough number of samples considered, the average K-asymmetry should be null and that the value for a sample that comprise a statistically large number of spheres should also be null. At the micro-scale, the rotatory character of the flow is shown by the

evolution of the averaged local vorticity (see Fig. A.8) which displays a larger amplitude at subsample sizes where K-asymmetry is considerable and decreases with increasing size. This illustrates intuitively the theoretical point that K-asymmetry induces rotatory flow.

3. Application to real microstructures

The previous section predicted the expected theoretical behaviour of granular porous media regarding the K-asymmetry. We now verify for real rocks if the natural heterogeneities, mostly included within grain shape properties, may change the results.
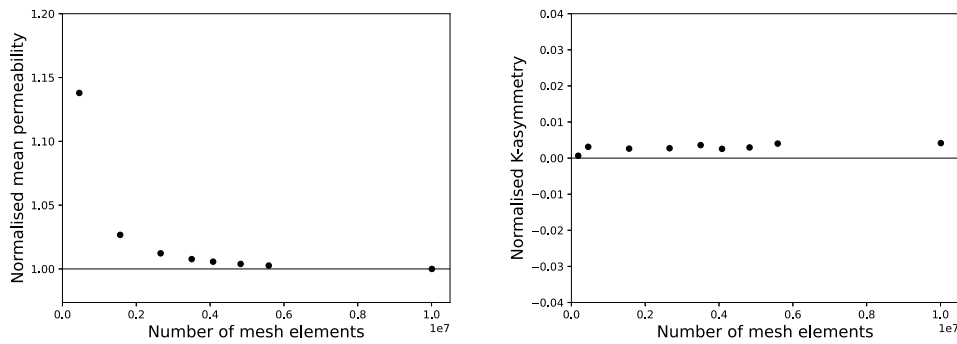
Fig. 3. Mesh convergence of the mean permeability of the 2D cross section shown in Fig. 1. The corresponding K-asymmetry is plotted in comparison.
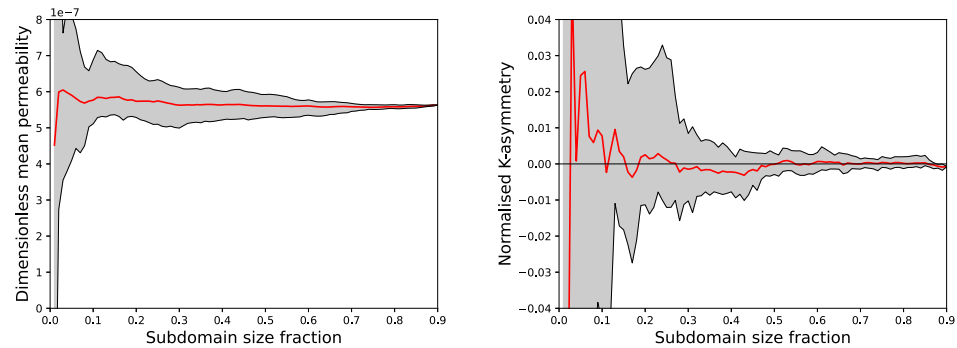

Fig. 4. REV convergence of the mean permeability and the K-asymmetry, for two RCP samples, including the one of Fig. 1. The range of values in each plot is highlighted in grey and the average value is plotted in red. The convergence is assessed by increasing the size fraction of the domain considered.

With this purpose in mind, this section focuses on the study of real rocks, digitised. The process of digital rock reconstruction applied follows Lesueur et al. (2017). Pixel data of a stack of segmented 2D microCT scan images of rock is translated to a 3D structured mesh of the rock's pore space onto which flow simulations can be run.

We consider two samples, selected on purpose at the two extremes of natural heterogeneity. The first one is the LV60 A sandpack (Imperial College Consortium On Pore-Scale Modelling, 2014b), shown in Fig. 5a. Sandpacks are made of real grains of sands artificially consolidated. While the grains themselves present classic heterogeneities of roughness and non-sphericity, the little consolidation pressure does not trigger much deformation of the grains. Being a monomineralic material, grain shape and size also remains fairly homogeneous. The pore space that can be observed in the figure is entirely connected throughout. As typical of sandpacks, Mostaghimi et al. (2012) showed that the LV60 A is essentially isotropic. On the other end of the spectrum, we selected a C2 carbonate (Imperial College Consortium On Pore-Scale Modelling, 2014a). Carbonate rocks are most commonly known for their high heterogeneity and this is displayed in Fig. 5b. Grain shapes and sizes vary considerably and the pore space displays many zones of non-connected porosity neighbouring large pores.

For these samples, we perform an REV convergence analysis, using the same approach described in Section 2.3. We perform the simulations with a mesh size twice the resolution of the image following the recommendation of Guibert et al. (2015b) for adequate mesh convergence. Similarly to the previous study, we consider two spatially independent samples for statistical representativeness. On each, four subsamples are selected for the analysis, growing from different corners (namely left-bottom-back/right-top-back/left-top-front/right-bottom-front). Again, an overlap starts at a subdomain relative size of ≈0.45, which will be discussed in the interpretation of the results.

Results for the LV60 A sandpack are plotted in Fig. 6. REV is globally reached past 0.8 after which the amplitude of permeability variation remains constant. We note that variations of the order of 10% are still present compared to the perfect convergence of the RCP which can

be explained by the natural heterogeneity of the medium. The values of permeability match with the ones obtained by Mostaghimi et al. (2012) with a similar method, where REV convergence was assessed at 1.1 mm (equivalent to a subdomain size fraction of 0.75 on Fig. 6). The three corresponding asymmetries (xy, xz and yz) are plotted in Fig. 6b. When the subdomains considered are too small, i.e. inferior to 0.1, the K-asymmetry values are random because the subsamples often do not percolate. However, past this threshold, a more regular cone of convergence is observed and each of the components reaches an REV at a final value close to zero. Note that the difference to zero could be an artefact due to the lack of data at high subdomain size fraction and therefore of statistical representation. Despite the REV value approaching zero as predicted by the RCP, we note that the cone of convergence of the K-asymmetry presents an amplitude five times bigger than the one of the RCP. We can conclude that heterogeneities of grain shape increase the magnitude of the K-asymmetry.

Results for the C2 carbonate are plotted in Fig. 7. Since the carbonate is not necessarily isotropic, we evaluate the permeability independently in its three directions instead of considering the mean value of the tensor's diagonal components. The most noticeable difference with the RCP and the sandpack is that some carbonate subsamples still do not percolate at a size fraction of 0.75. Therefore, a cone of convergence does not exist until then and the window remaining between 0.75 to 0.9 is at that point too small to predict any convergence. Still, the final value of permeability obtained in the x-direction matches the one from Mostaghimi et al. (2012). Mostaghimi et al. (2012) themselves did not find any REV for the sample even at a size of 1.6 mm. The corresponding K-asymmetry also differs from the RCP and the sandpack. The K-asymmetry starts to stabilise only past a size fraction of 0.5. At this point, the envelope of K-asymmetry values has an amplitude five times larger than the sandpack's when its K-asymmetry stabilised (at a size fraction of 0.3 on Fig. 6). The range of K-asymmetry then narrows down slowly until the consideration of the full domain, noting that the overlapping of subsamples past 0.7 should dissuade us from over-interpreting those results. Indeed, the final value obtained on a full
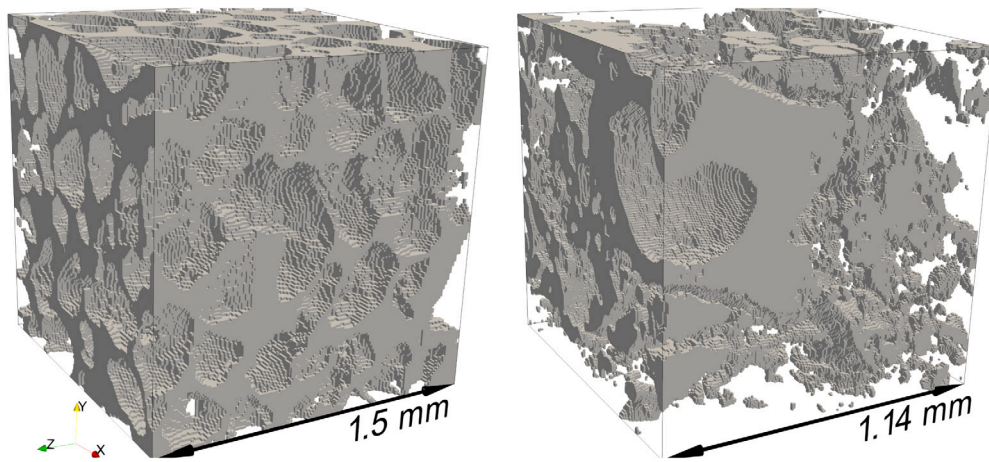
Fig. 5. Pore space of the LV60 A sandpack (left) and C2 carbonate (right) samples.
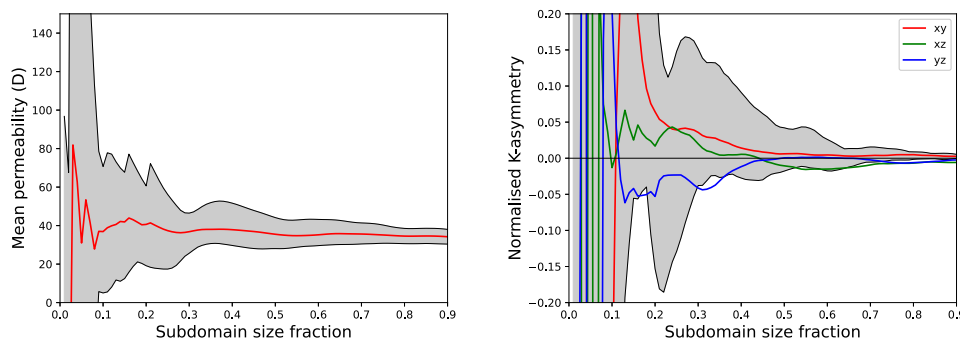

Fig. 6. REV convergence of the mean permeability and the K-asymmetry, for two sandpack samples, including the one of Fig. 5a. The full cubic sample has a size of 1.5 mm. For visualisation purposes, only the range of K-asymmetry values for the *xy* component is plotted.
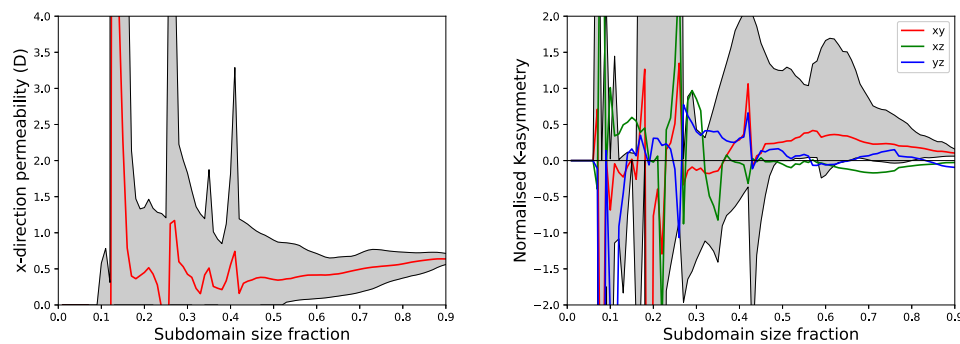

Fig. 7. REV convergence of the permeability in the x-direction and the K-asymmetry, for two carbonate samples, including the one of Fig. 5b. The full cubic sample has a size of 1.14 mm. For visualisation purposes, only the range of K-asymmetry values for the *xy* component is plotted.

domain analysis reduces down to a statistic from two samples. While we can assess without a doubt that the K-asymmetry average value has stabilised, an REV of K-asymmetry has definitely not been reached and no prediction can be made on the size of the REV. Interestingly, the final value corresponds to 50 times the one of the sandpack and 150 times of the RCP.

In conclusion, this analysis shows that the K-asymmetry of real rocks — when it exists — still vanishes past the REV size. Yet, natural heterogeneities such as grain shape and size distribution contribute to a large K-asymmetry increase up to that point.

4. Conclusion

When scale separation is not present, asymmetry of the permeability tensor at the micro-scale is meant to exist. The physical justification lies

in the fact that tortuous paths through discretised grains can randomly affect the flow direction. With proper homogenisation, we recover the symmetry at REV size, which reconciles with upscaling theories, since statistically speaking, asymmetry has equal chances to produce a deviation in any direction. This was demonstrated in our statistical study where the average value of asymmetry remained approximately null, enveloped by a cone of convergence narrowing down to zero as it reaches the REV size. We note that the REV size of asymmetry may be larger than the REV size of the diagonal components of the permeability tensor, as it also depends on the off-diagonal components.

This study puts to rest the concept that asymmetry is purely a numerical error. Even though individual components of the permeability tensor follow a normal mesh convergence, the asymmetry itself does not necessarily decrease when numerical error is reduced. Even though asymmetry can be numerically reduced with finer meshes because
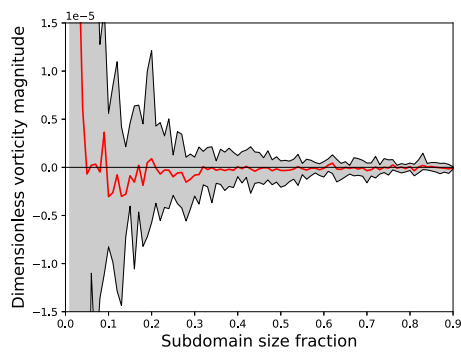
Fig. A.8. REV convergence of the flow local vorticity for two RCP samples, including the one of Fig. 1, computed for one of the flow directions. The range of values in each plot is highlighted in grey and the average value is plotted in red.

Appendix. Vorticity

To evaluate the rotary character of the flow, we compute the local vorticity of the fluid velocity field and plot the statistical REV convergence of its averaged magnitude in Fig. A.8.

individual components of the permeability tensor follow a normal mesh convergence, its existence below REV size is natural. Still, even with a supposedly unfavourable type of boundary conditions prescribed (Guibert et al., 2015a), we prove that the symmetry is recovered at REV size — away from the boundary as Thovert and Mourzenko (2020) recommends. Based on the latter study, we suggest this result holds for any type of boundary conditions. As detailed in this work, the existence of an anti-symmetric part of the permeability tensor indicates that the domain considered may simply not satisfy scale separation and/or representativeness. Numerical homogenisation methods trying to force the symmetry may hide the fact that either some fundamental REV assumptions behind Darcy's law are not always satisfied or the boundary layer is mistakenly included. As detailed in this work, the existence of an anti-symmetric part of the permeability tensor indicates that the domain considered may simply not satisfy scale separation and/or representativeness.

Finally, the presence of natural heterogeneities in rocks such as grain shape and size was shown to drastically increase the asymmetry compared to an assemblage of perfectly round spheres. However, that asymmetry still vanishes past the REV size. Interestingly, as we transition through the scales, asymmetry may reappear due to the presence of new heterogeneities in the rock (Veveakis and Regenauer-Lieb, 2015), such as fractures, as it was shown that fracture networks can produce asymmetrical permeability tensor as well.

CRediT authorship contribution statement

Martin Lesueur: Conceptualization, Methodology, Software, Investigation, Writing. **Alexandre Guével:** Conceptualization, Writing. **Thomas Poulet:** Conceptualization, Methodology, Software, Writing.

Declaration of competing interest

The authors declare that they have no known competing financial interests or personal relationships that could have appeared to influence the work reported in this paper.

Data availability

Data will be made available on request.

Acknowledgements

References

Auriault, J., 1991. Heterogeneous medium. Is an equivalent macroscopic description possible? Internat. J. Engrg. Sci. 29 (7), 785–795. http://dx.doi.org/10.1016/0020-7225(91)90001-j.

Auriault, J.-L., Geindreau, C., Royer, P., 2000. Filtration law in rotating porous media. C. R. De L'académie Des Sci. - Ser. IIB - Mechanics 328 (11), 779–784. http://dx.doi.org/10.1016/s1620-7742(00)01261-7.

Baghbanan, A., Jing, L., 2007. Hydraulic properties of fractured rock masses with correlated fracture length and aperture. Int. J. Rock Mech. Min. Sci. 44 (5), 704–719. http://dx.doi.org/10.1016/j.ijrmms.2006.11.001.

Beard, D.C., Weyl, P.K., 1973. Influence of texture on porosity and permeability of unconsolidated sand. AAPG Bull. 57, http://dx.doi.org/10.1306/819a4272-16c5-11d7-8645000102c1865d.

Blunt, M.J., Bijeljic, B., Dong, H., Gharbi, O., Iglauer, S., Mostaghimi, P., Paluszny, A., Pentland, C., 2013. Pore-scale imaging and modelling. Adv. Water Resour. 51, 197–216. http://dx.doi.org/10.1016/j.advwatres.2012.03.003.

Cox, M.R., Budhu, M., 2008. A practical approach to grain shape quantification. Eng. Geol. 96 (1–2), 1–16. http://dx.doi.org/10.1016/j.enggeo.2007.05.005.

Durlofsky, L.J., 1991. Numerical calculation of equivalent grid block permeability tensors for heterogeneous porous media. Water Resour. Res. 27 (5), 699–708. http://dx.doi.org/10.1029/91wr00107.

Dvorkin, J., Armbruster, M., Baldwin, C., Fang, Q., Derzhi, N., Gomez, C., Nur, B., Nur, A., 2008. The future of rock physics: Computational methods vs. lab testing. First Break 26 (9), http://dx.doi.org/10.3997/1365-2397.26.1292.28600.

Gerke, K.M., Karsanina, M.V., Katsman, R., 2019. Calculation of tensorial flow properties on pore level: Exploring the influence of boundary conditions on the permeability of three-dimensional stochastic reconstructions. Phys. Rev. E 100 (5), 053312. http://dx.doi.org/10.1103/physreve.100.053312.

Geuzaine, C., Remacle, J.-F., 2009. GMSH: A 3-D finite element mesh generator with built-in pre- and post-processing facilities. Internat. J. Numer. Methods Engrg. 79 (11), 1309–1331. http://dx.doi.org/10.1002/nme.2579.

Guibert, R., Horgue, P., Debenest, G., Quintard, M., 2015a. A comparison of various methods for the numerical evaluation of porous media permeability tensors from pore-scale geometry. Math. Geosci. 48 (3), 329–347. http://dx.doi.org/10.1007/s11004-015-9587-9.

Guibert, R., Nazarova, M., Horgue, P., Hamon, G., Creux, P., Debenest, G., 2015b. Computational permeability determination from pore-scale imaging: Sample size, mesh and method sensitivities. Transp. Porous Media 107 (3), 641–656. http://dx.doi.org/10.1007/s11242-015-0458-0.

Imperial College Consortium On Pore-Scale Modelling, 2014a. C2 carbonate. http://dx.doi.org/10.6084/M9.FIGSHARE.1189258.V1, figshare.

Imperial College Consortium On Pore-Scale Modelling, 2014b. LV60A Sandpack. http://dx.doi.org/10.6084/m9.figshare.1153795.

King, M., 1993. Application and analysis of Tensor permeability to crossbedded reservoirs. In: All Days. SPE, http://dx.doi.org/10.2118/26118-ms.

Koch, D.L., Brady, J.F., 1987. The symmetry properties of the effective diffusivity tensor in anisotropic porous media. Phys. Fluids 30 (3), 642. http://dx.doi.org/10.1063/1.866368.

Lang, P.S., Paluszny, A., Zimmerman, R.W., 2014. Permeability tensor of three-dimensional fractured porous rock and a comparison to trace map predictions. J. Geophys. Res.: Solid Earth 119 (8), 6288–6307. http://dx.doi.org/10.1002/2014jb011027.

Lasseux, D., Valdés-Parada, F.J., 2017. Symmetry properties of macroscopic transport coefficients in porous media. Phys. Fluids 29 (4), 043303. http://dx.doi.org/10.1063/1.4979907.

Lesueur, M., Casadiego, M.C., Veveakis, M., Poulet, T., 2017. Modelling fluid-microstructure interaction on elasto-visco-plastic digital rocks. Geomech. Energy Environ. 12, 1–13. http://dx.doi.org/10.1016/j.gete.2017.08.001.

Long, J.C.S., Remer, J.S., Wilson, C.R., Witherspoon, P.A., 1982. Porous media equivalents for networks of discontinuous fractures. Water Resour. Res. 18 (3), 645–658. http://dx.doi.org/10.1029/wr018i003p00645.

Manwart, C., Aaltosalmi, U., Koponen, A., Hilfer, R., Timonen, J., 2002. Lattice-Boltzmann and finite-difference simulations for the permeability for three-dimensional porous media. Phys. Rev. E 66 (1), 016702. http://dx.doi.org/10.1103/physreve.66.016702.

Marafini, E., Rocca, M.L., Fiori, A., Battiato, I., Prestininzi, P., 2020. Suitability of 2D modelling to evaluate flow properties in 3D porous media. Transp. Porous Media 134 (2), 315–329. http://dx.doi.org/10.1007/s11242-020-01447-4.

Mostaghimi, P., Blunt, M.J., Bijeljic, B., 2012. Computations of absolute permeability on micro-CT images. Math. Geosci. 45 (1), 103–125. http://dx.doi.org/10.1007/s11004-012-9431-4.

Pouya, A., Fouché, O., 2009. Permeability of 3D discontinuity networks: New tensors from boundary-conditioned homogenisation. Adv. Water Resour. 32 (3), 303–314. http://dx.doi.org/10.1016/j.advwatres.2008.08.004.

Romano, P.K., Horelik, N.E., Herman, B.R., Nelson, A.G., Forget, B., Smith, K., 2015. OpenMC: A state-of-the-art Monte Carlo code for research and development. Ann. Nucl. Energy 82, 90–97. http://dx.doi.org/10.1016/j.anucene.2014.07.048.

Sagar, B., Runchal, A., 1982. Permeability of fractured rock: Effect of fracture size and data uncertainties. Water Resour. Res. 18 (2), 266–274. http://dx.doi.org/10.1029/wr018i002p00266.

Sanchez-Palencia, E., 1982. On the asymptotics of the fluid flow past an array of fixed obstacles. Internat. J. Engrg. Sci. 20 (12), 1291–1301. http://dx.doi.org/10.1016/0020-7225(82)90055-6.

Sedaghat, M., Azizmohammadi, S., Matthäi, S.K., 2019. Does the symmetry of absolute permeability influence relative permeability tensors in naturally fractured rocks? J. Petrol. Explor. Prod. Technology 10 (2), 455–466. http://dx.doi.org/10.1007/s13202-019-00756-9.

Stokes, G., 1851. On the conduction of heat in crystals. Camb. Dublin Math. J. 6, 215–238.

Stroud, D., 1998. The effective medium approximations: Some recent developments. Superlattices Microstruct. 23 (3–4), 567–573. http://dx.doi.org/10.1006/spmi.1997.0524.

Thovert, J.-F., Mourzenko, V.V., 2020. On the influence of boundary conditions when determining transport coefficients from digital images of heterogeneous media. Adv. Water Resour. 141, 103612. http://dx.doi.org/10.1016/j.advwatres.2020.103612.

Torskaya, T., Shabro, V., Torres-Verdín, C., Salazar-Tio, R., Revil, A., 2013. Grain shape effects on permeability, formation factor, and capillary pressure from pore-scale modeling. Transp. Porous Media 102 (1), 71–90. http://dx.doi.org/10.1007/s11242-013-0262-7.

Truesdell, C., 1984. Rational Thermodynamics. Springer New York, New York, NY.

Veveakis, E., Regenauer-Lieb, K., 2015. Review of extremum postulates. Curr. Opin. Chem. Eng. 7, 40–46. http://dx.doi.org/10.1016/j.coche.2014.10.006.

Zhang, D., Zhang, R., Chen, S., Soll, W.E., 2000. Pore scale study of flow in porous media: Scale dependency, REV, and statistical REV. Geophys. Res. Lett. 27 (8), 1195–1198. http://dx.doi.org/10.1029/1999gl011101.

Zijl, W., Stam, J.M.T., 1992. Modeling permeability in imperfectly layered porous media. I. Derivation of block-scale permeability tensor for thin grid-blocks. Math. Geol. 24 (8), 865–883. http://dx.doi.org/10.1007/bf00894656.